Dual electro-optic frequency comb spectroscopy using pseudo-random modulation

KHAOULA FDIL[1,*], VINCENT MICHAUD-BELLEAU[1], NICOLAS BOURBEAU HÉBERT[1], PHILIPPE GUAY[1], ADAM J. FLEISHER[3], JEAN-DANIEL DESCHÊNES[2], AND JÉRÔME GENEST[1]

[1] *Centre d'optique, photonique et laser, Université Laval, Québec, Québec G1V 0A6, Canada*
[2] *OctoSig, Québec, Canada*
[3] *National Institute of Standards and Technology, 100 Bureau Drive, Gaithersburg, Maryland 20899, USA*
[*] *Corresponding author: khaoula.fdil.1@ulaval.ca*

Compiled July 4, 2019

An approach for dual-comb spectroscopy using electro-optic (EO) phase modulation is reported. Maximum-length pseudo-random binary sequences allow for energy-efficient and flexible comb generation. Self-correction of interferograms is shown to remove relative comb drifts and improve mutual coherence, even for EO combs derived from the same laser source. Methane spectroscopy is reported over a ∼10 GHz spectral range, limited by the modulators' bandwidth. The potential of a simple EO comb instrument is demonstrated to rapidly quantify atmospheric methane emissions with sub-ppm precision.

http://dx.doi.org/10.1364/ao.XX.XXXXXX

The detection and quantification of diffuse greenhouse gases and their respective sources and sinks represent an application of frequency comb spectroscopy [1–4]. Over conventional mode-locked laser sources, electro-optic (EO) combs [5] particularly offer several advantages, thanks to their simplicity, frequency-agility, and robustness. When the monitored gas is known *a priori* (e.g. methane), the spectral coverage of an EO comb can be matched to a single absorption feature. It thus provides an efficient distribution of multiplexed optical power for sensing. Subsequently, rapid read-out techniques such as frequency comb interference spectroscopy (FCIS) can enable down-mixing of the probing optical comb to electrical frequencies [6–8].

In that particular context, using a pseudo-random binary sequence (PRBS) phase modulation is known to achieve efficient comb generation, enabling real-time characterization of atomic dynamics for instance [9–11]. However, because FCIS does not benefit from a spectral compression while converting from optical to electrical frequencies, it requires multi-gigahertz detection chains to acquire molecular absorption features at typical atmospheric pressure [5]. Chirped-pulse EO comb spectroscopy [12, 13] displays similar advantages and limitations. To allow for a slower and less expensive acquisition system, a dual EO comb approach can be employed. However, this forces compromises on the measurement duration or the achievable signal-to-noise ratio (SNR) [14].

In this Letter, we propose and demonstrate a new kind of dual EO comb spectrometer which uses two PRBS modulating at slightly detuned rates, to generate independent EO combs originating from a single CW laser source. Maximum-length sequences (MLS) are used to maximize the spectral flatness of the EO combs. Even if the generated EO combs derived from the same CW laser display intrinsically high mutual coherence, it is shown that interferogram self-correction [15] is an effective approach to improve coherent averaging.

The simple spectrometer design uses only a semiconductor laser and fiber-based components which are readily integrable into a small, field-deployable package. Methane is used here as a target gas to evaluate instrument performance, and further to show that dual EO combs could be used to quantify atmospheric regional methane emissions as in [4], but with a lower cost per station and at a projected precision of 5 ppb at a hypothetical open-path length of 1 km.

The experimental setup is shown in Fig. 1. The output of a distributed feedback laser diode at 1654 nm (NTT NLK1U5FAAA) was split in two paths, each containing a phase modulator (EOSpace PM-085-20-PFA-PFA-1550/1650), with 10 GHz nominal bandwidth. PRBS were generated using two Xilinx VC707 field-programmable gate array (FPGA) demonstration boards that were clocked at two distinct, but phase-coherent, frequencies using a two-channel direct digital synthesizer (DDS) (Analog Devices AD9958/59 Evaluation board Z Rev. C) .

The VC707s were clocked at 200.00 MHz and 200.05 MHz and each used an on-board high-speed serial transmitter (GTX) that generated bits at 50 times the seeded clock rate such that bit streams were at $f_{bit} = 10.0000$ GHz and 10.0025 GHz respectively. Since sequences of length $N = 2^9 - 1 = 511$ bits were used, the pattern repetition rate was $f_r = f_{bit}/N = 19.57$ MHz, with a difference of $\Delta f_r = 4.89$ kHz between the two combs. The electrical signals were amplified (modulator drivers JDSU H301-1210) to drive the phase modulators near the V_π condition.

To maximize the spectral flatness of the generated EO combs, MLS were used [9] as pseudo-random signals. Assuming perfectly square bits, the amplitudes of the PRBS harmonics then follow a cardinal sine envelope, with a first zero at $f_{bit} = 10$ GHz in our case, as shown in Fig. 2 (red line). A full optical bandwidth of approximately 15 GHz is thus theoretically available for

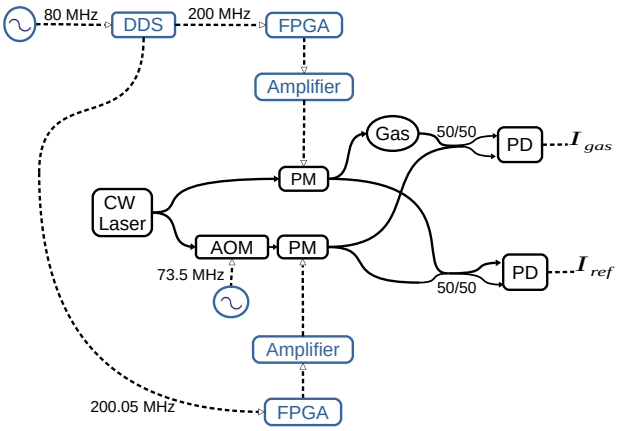

Fig. 1. Experimental setup for dual PRBS EO comb spectroscopy. Solid lines represent fiber links, dashed lines represent electrical links. Fiber-optic splitters/combiners have a 50/50 power ratio. DDS: Direct digital synthesis, FPGA: Field-programmable gate array, AOM: Acousto-optic modulator, PM: Phase modulator, Gas: methane cell, PD: Photodetectors (Thorlabs PDB430C).

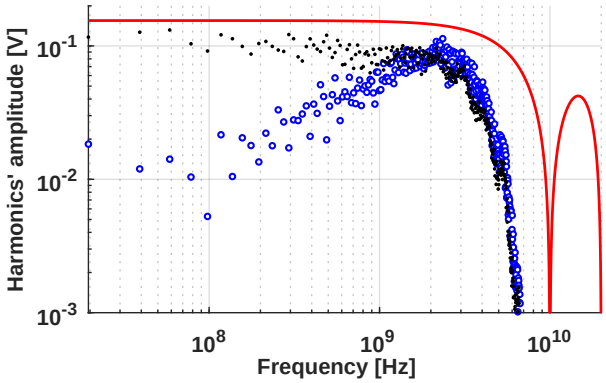

Fig. 2. Harmonic spectra at the output of the modulator drivers, acquired during 3.2 ms with a 4 GHz bandwidth oscilloscope having a 40 GS/s sampling frequency. The two MLS are generated by the two FPGAs and amplified by the two modulator drivers (JDSU H301-1210). The blue circles and the black dots represent the harmonics' amplitude of these two MLS. The solid line is the Fourier series of the theoretical MLS. The MLS have a length of $2^9 - 1 = 511$, a repetition rate of 19.57 MHz and a bit frequency of 10 GHz.

spectroscopy, using appropriate equipment. As seen in Fig. 2, above 4 GHz the experimental curves deviate noticeably from the theoretical cardinal sine. This stems not only from the bandwidth limitations of the VC707 boards and modulator drivers, but also from the bandwidth of the oscilloscope used for the measurement. It can be noted that one modulator driver (blue curve) has an unexplained high-pass behavior, resulting in less power in the harmonics below 1 GHz.

The desired PRBS were generated offline and loaded to the FPGAs which were programmed to repeatedly loop through the sequences. The GTX high-speed serial transmitters on the VC707 boards allowed adjustable amplitude, pre-emphasis, and post-emphasis. These parameters were modified experimentally so as to optimize the spectral flatness. The optimal conditions depend upon the specific phase modulators and amplifiers used. For the measurements presented here, the parameters were set to 280 mV_{pp}, 3 dB, and 3 dB respectively.

In the experimental setup (Fig. 1), it can be seen that an acousto-optic frequency shifter is used on the second comb signal. Since the repetition rate is $f_r = 19.57$ MHz, the AOM frequency $f_{AOM} = 73.5$ MHz shifts the beating signal by more than $3f_r$ (panel A of Fig. 3). However, as a dual comb contains 2 beating signals per f_r spectral interval (panel B of Fig. 3), there is one alias at $f_{AOM} - 3f_r = 14.79$ MHz as well as one at $4f_r - f_{AOM} = 4.78$ MHz.

After the phase-modulation, the first comb was used to probe a (5.5 ± 0.1) cm-long methane cell under a pressure of (98.7±9.9) kPa. The light at the cell's output was mixed with the second comb using a 50/50 coupler. The second comb thus acted as a local oscillator allowing the retrieval of the gas spectrum in phase as well as in amplitude.

A second interferometer, in which neither of the combs interrogated the sample, was also used to simultaneously provide a reference measurement for spectral normalization [16]. This method was chosen to mitigate the impact of time variations in the modulation patterns. After detection, the two interferograms I_{gas} and I_{ref} were low-pass filtered at 22 MHz (Minicircuit BLP-21.4+) and digitized with a GaGe compuScope (CSE8389) acquisition card at $f_s = 50$ MS/s for a total duration of 10 seconds. The digitized interferograms were first band-pass filtered to keep only the alias around 4.78 MHz. This spectral copy was next demodulated numerically, cancelling the AOM frequency shift and yielding a complex signal which only preserved the spectral alias closest to DC.

Self-correction was applied to the probe and reference interferograms independently. In each case, the first interferogram was used as a template which was cross-correlated with the full signal. This allowed retrieving the evolution of the interferogram periodicity and phase, with a Δf_r sampling rate. As in [17], the phase information was interpolated to phase-correct each sample of the interferograms and the periodicity information was used to resample the interferograms such that each period exactly contained the same integer number of samples. Each repetition period could then easily be segmented and they all could be averaged before computing the Fourier transform.

The evolution of the periodicity information as well as the phase over a 10-second measurement is shown in the Fig. 4. Panel A shows the offset of each uncorrected interferogram relative to its expected timing, in number of samples. The linear relation indicates that the 52446 interferograms have accumulated 330 more points than expected. In other words, instead of holding exactly $f_s/\Delta f_r = 10220$ points, each interferogram displayed an extra $\sim 6/1000$ of a point. This is chiefly explained by the absence of synchronization between the sampling oscilloscope and the DDS. However, synchronization would not have completely solved the issue since, because of quantization, the two synthesizers could not produce the perfectly integer $f_r/\Delta f_r$ that was required. Panel B shows the unwrapped phase ramp which arises from the fact that the 4.78 MHz downshift did not bring the spectral alias' central tooth exactly to zero. This ramp could be easily identified and corrected, yielding the residual phase shown in panel C. This residual phase was different for the probe and reference measurements and was mostly due to independent fiber drifts in those two distinct interferometers.

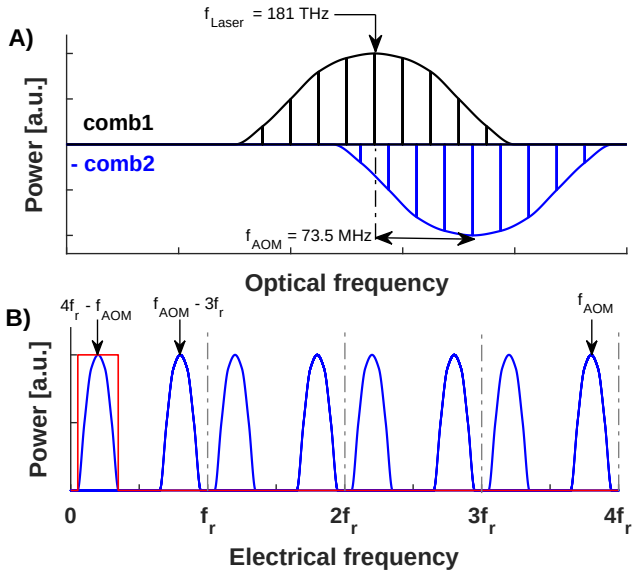

Fig. 3. A) Two optical combs with two different repetition rates: $f_r = 19.57$ MHz and $f_r + \Delta f_r = 19.57 + 0.005$ MHz and an AOM-induced frequency shift larger than $3f_r$. B) The beating of the two optical combs in A). The red line is the band-pass filter used to isolate the chosen spectral alias.

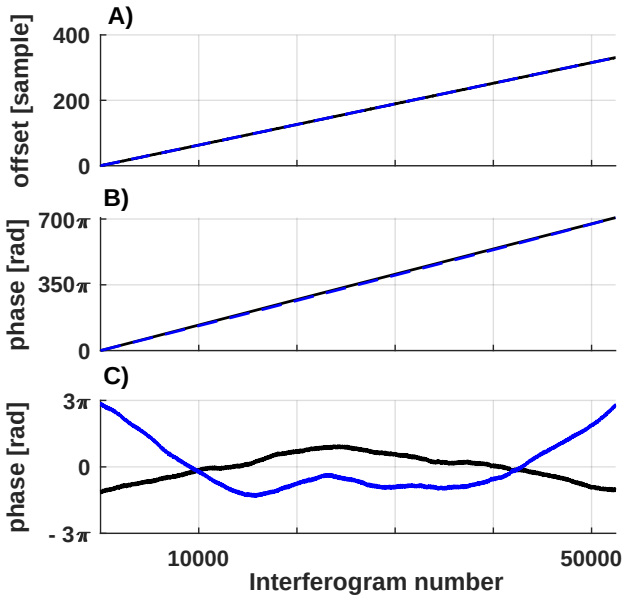

Fig. 4. A) Offset of each interferogram relative to their expected timing. B) Unwrapped phase before AOM shift cancellation. C) Residual phase after AOM shift cancellation. Black curves are for the probe interferometer. Blue curves are for the reference interferometer.

This highlights the fact that interferogram correction is needed even when the two combs are highly mutually stable since perturbations downstream of the laser source can easily impact the interferograms' phase evolution.

The probe and reference signals were phase-corrected, resampled, averaged and Fourier transformed. The complex ratio of the resulting spectra was then computed to retrieve the complex transmission spectrum of the gas sample. The modulus and the phase of the computed transmission compared to a fitted model are shown in Fig. 5 . The fit comprised a sum of Voigt profiles whose initial parameters were taken from the HITRAN 2016 database [18]. For this optimization, the temperature was fixed at 20.8°C. The adjustable parameters were the pressure (P), the cell length (L), the absolute frequency, and two different linear baselines for the modulus and the phase. Fitting the absolute frequency was needed because the CW laser frequency was not known *a priori* with sufficient accuracy. The linear baselines took into account varying spectral discrepancies between the probe and reference channels. The modulus and the phase were fitted simultaneously. The retrieved gas cell parameters were: $P = (94 \pm 2.7)$ kPa and $L = (5.51 \pm 0.8)$ cm. The uncertainties correspond to the 95% confidence intervals returned by the fit.

The residuals (Fig. 5) show some systematic structure, which is consistent with known shortcomings of the chosen spectral model comprising a sum of Voigt profiles (e.g., speed-dependent collisions, line mixing, etc.). The increased noise, around an electronic offset of 0 MHz, is explained by the lower power per comb tooth in one of the PRBS combs discussed earlier (Fig. 2). Similarly, the increased random residuals at the edges (± 1 MHz), are explained by the limited optical bandwidth of the modulator drivers (Fig. 2). Importantly, the local baseline noise throughout the remainder of the spectrum is ≈ 0.001 at the 10-second integration time.

Using the observed noise level, a projected precision was estimated for atmospheric CH_4 mole fraction retrieval of $\sigma = 5$ ppb at an open-path length of $L = 1$ km. The projected open-path sensing precision was calculated by fitting simulated complex-valued spectra of atmospheric CH_4 ($\chi_{CH_4} = 1.8$ ppm, $L = 1$ km, $T = 296$ K) with absorbance noise of 0.001 (0.001 rad for the phase), sampled at an optical frequency spacing of $f_r = 15$ MHz. The fitted model retrieved the absolute frequency, pressure, mole fraction, and the standard deviation of the fitted mole fraction for 100 independent simulations. The model yielded the estimated open-path sensing precision of $\sigma = 5$ ppb.

The PRBS comb bandwidth, as illustrated in Fig. 5, was well matched to the entire CH_4 absorption feature near 1653.73 nm. Consequently, nearly all the EO comb teeth provided simultaneously independent measurements of the sample gas. The projected precision, for open-path sensing of mole fraction, is therefore significantly better than the traditional single-frequency figures of merit (e.g., noise-equivalent absorption), which is routinely discussed for continuous-wave laser sensors. Hence, for relatively narrow-band spectroscopy, EO combs coupled with fast and programmable interferometric read-out techniques represent a promising new architecture for robust field-deployable sensors.

The SNR evolution, as a function of the number of averaged interferograms for both the raw and corrected signals, is shown in Fig. 6. The raw averaging accounts for the fractional number of points per interferogram, but not for the extraneous Δf_r and phase fluctuations. This was done to reflect an experimental case where all frequencies are synchronized to enforce the so-called coherent averaging condition. Still, it can clearly be seen in Fig. 6 that coherent averaging begins to fail at time scales longer than 2 seconds for uncorrected signal. Meanwhile, self correction allows retrieving the mutual coherence between the two sources at time scales longer than 10 seconds, limited by our acquisition duration. This demonstrates that software self

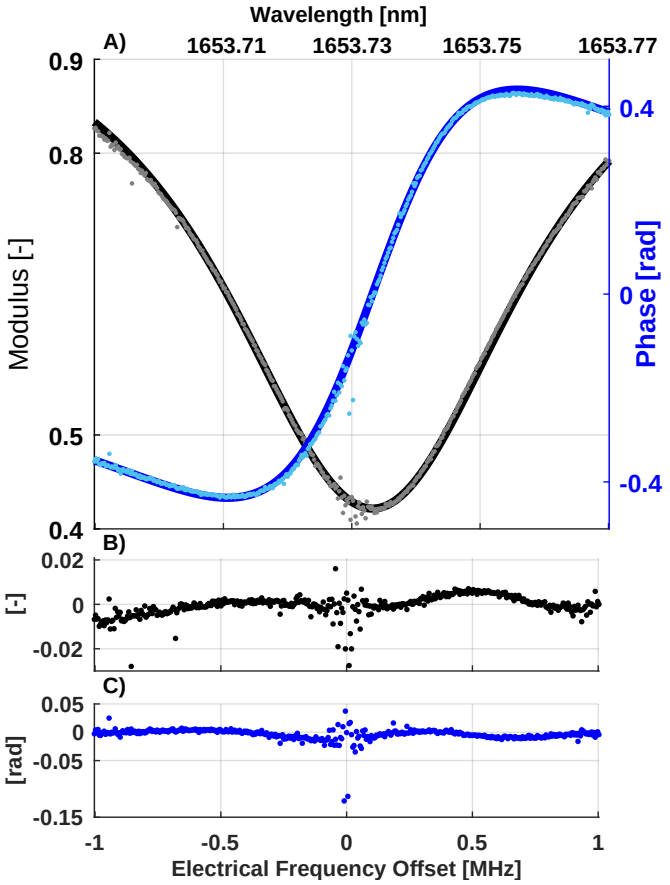

Fig. 5. Complex transmission spectrum of methane near 1653.73 nm. A) The black and the grey curves represent the modulus and the blue curves represent the phase. Experimental data points are plotted as dots. The fitted model computed with parameters from the HITRAN 2016 database is plotted as solid lines. The compression factor from optical to electrical frequencies is 4000. B) Modulus residuals. C) Phase residuals.

correction is beneficial even for highly mutually coherent dual EO comb systems.

In summary, this Letter proposes an approach for dual EO comb spectroscopy using pseudo-random binary sequences. Maximal-length sequences are used for maximizing the spectral flatness. Interferogram self-correction is a necessary processing approach to implement coherent averaging, despite the use of highly mutually coherent combs. The technique, demonstrated here using a methane cell, exhibited residual noise levels commensurate with detecting atmospheric methane with a precision of 5 ppb over a hypothetical open-path length of 1 km with a simple, inexpensive, and robust instrument.

FUNDING.

The authors would like to acknowledge financial support from the Natural Sciences and Engineering Research Council of Canada (NSERC).

ACKNOWLEDGEMENT.

Certain commercial equipment is identified in the paper in order to specify the experimental procedure adequately. Such identification is not intended to imply recommendation or endorsement by the National Institute of Standards and Technology, nor is it intended to imply that the equipment identified is necessarily the best available for the purpose.

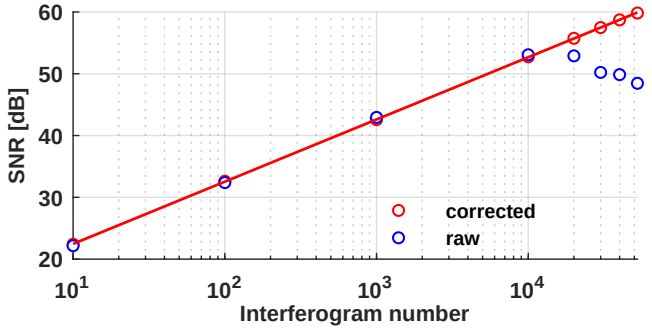

Fig. 6. Evolution of the spectral SNR during the 10-second measurement. The circles represent the computed SNR values for corrected (red) and raw (blue) data corresponding to the reference signal I_{ref}. Theses values are similar to the SNR retrieved in the probe signal. The solid line represents a linear fit of the SNR for corrected data. Its slope is 10 dB/decade.

REFERENCES

1. G. B. Rieker, F. R. Giorgetta, W. C. Swann, J. Kofler, A. M. Zolot, L. C. Sinclair, E. Baumann, C. Cromer, G. Petron, C. Sweeney, P. P. Tans, I. Coddington, and N. R. Newbury, Optica **1**, 290 (2014).
2. S. Coburn, C. B. Alden, R. Wright, K. Cossel, E. Baumann, G.-W. Truong, F. Giorgetta, C. Sweeney, N. R. Newbury, K. Prasad, I. Coddington, and G. B. Rieker, Optica **5** (2017).
3. S. Schmitt, D. Pöhler, U. Platt, S. Hammer, D. W. T. Griffith, and S. Vardag, Atmospheric Meas. Tech. **11** (2018).
4. C. B. Alden, S. Ghosh, S. Coburn, C. Sweeney, A. Karion, R. Wright, I. Coddington, G. B. Rieker, and K. Prasad, Atmospheric Meas. Tech. **11**, 1565 (2018).
5. P. Martín-Mateos and P. Acedo, "Electro-optic dual optical frequency combs outside of the metrology lab: Opportunities in and beyond spectroscopy," in *CLEO Pacific Rim Conference 2018,* (Optical Society of America, 2018), p. W4F.1.
6. K. Urabe and O. Sakai, Appl. Phys. Lett. **101**, 051105 (2012).
7. K. Urabe and O. Sakai, Phys. Rev. A **88**, 023856 (2013).
8. J.-D. Deschênes and J. Genest, Appl. Opt. **53**, 731 (2014).
9. N. B. Hébert, V. Michaud-Belleau, J. D. Anstie, J.-D. Deschênes, A. N. Luiten, and J. Genest, Opt. Express **23**, 27806 (2015).
10. N. B. Hébert, V. Michaud-Belleau, C. Perrella, G.-W. Truong, J. D. Anstie, T. M. Stace, J. Genest, and A. N. Luiten, Phys. Rev. Appl. **6**, 044012 (2016).
11. N. Wilson, N. B. Hébert, C. Perrella, P. Light, J. Genest, S. Pustelny, and A. Luiten, Phys. Rev. Appl. **10**, 034012 (2018).
12. D. A. Long, A. J. Fleisher, D. F. Plusquellic, and J. T. Hodges, Phys. Rev. A **94**, 061801 (2016).
13. D. A. Long, A. J. Fleisher, D. F. Plusquellic, and J. T. Hodges, Opt. Lett. **42**, 4430 (2017).
14. I. Coddington, N. Newbury, and W. Swann, Optica. **3**, 414 (2016).
15. N. B. Hébert, J. Genest, J.-D. Deschênes, H. Bergeron, G. Y. Chen, C. Khurmi, and D. G. Lancaster, Opt. Express **25**, 8168 (2017).
16. D. A. Long, A. J. Fleisher, K. O. Douglass, S. E. Maxwell, K. Bielska, J. T. Hodges, and D. F. Plusquellic, Opt. Lett. **39**, 2688 (2014).
17. P. Guay, J. Genest, and A. J. Fleisher, Opt. Lett. **43**, 1407 (2018).
18. I. E. Gordon, L. S. Rothman, C. Hill, R. V. Kochanov, Y. Tan, P. F. Bernath, M. Birk, V. Boudon, A. Campargue, K. Chance *et al.*, J. Quant. Spectrosc. Radiat. Transf. **203**, 3 (2017).

FULL REFERENCES

1. G. B. Rieker, F. R. Giorgetta, W. C. Swann, J. Kofler, A. M. Zolot, L. C. Sinclair, E. Baumann, C. Cromer, G. Petron, C. Sweeney, P. P. Tans, I. Coddington, and N. R. Newbury, "Frequency-comb-based remote sensing of greenhouse gases over kilometer air paths," Optica. **1**, 290–298 (2014).
2. S. Coburn, C. B. Alden, R. Wright, K. Cossel, E. Baumann, G.-W. Truong, F. Giorgetta, C. Sweeney, N. R. Newbury, K. Prasad, I. Coddington, and G. B. Rieker, "Continuous regional trace gas source attribution using a field-deployed dual frequency comb spectrometer," Optica. **5** (2017).
3. S. Schmitt, D. Pöhler, U. Platt, S. Hammer, D. W. T. Griffith, and S. Vardag, "Long open-path measurements of greenhouse gases in air using near-infrared fourier transform spectroscopy," Atmospheric Meas. Tech. **11** (2018).
4. C. B. Alden, S. Ghosh, S. Coburn, C. Sweeney, A. Karion, R. Wright, I. Coddington, G. B. Rieker, and K. Prasad, "Bootstrap inversion technique for atmospheric trace gas source detection and quantification using long open-path laser measurements," Atmospheric Meas. Tech. **11**, 1565–1582 (2018).
5. P. Martín-Mateos and P. Acedo, "Electro-optic dual optical frequency combs outside of the metrology lab: Opportunities in and beyond spectroscopy," in *CLEO Pacific Rim Conference 2018,* (Optical Society of America, 2018), p. W4F.1.
6. K. Urabe and O. Sakai, "Absorption spectroscopy using interference between optical frequency comb and single-wavelength laser," Appl. Phys. Lett. **101**, 051105 (2012).
7. K. Urabe and O. Sakai, "Multiheterodyne interference spectroscopy using a probing optical frequency comb and a reference single-frequency laser," Phys. Rev. A **88**, 023856 (2013).
8. J.-D. Deschênes and J. Genest, "Frequency-noise removal and on-line calibration for accurate frequency comb interference spectroscopy of acetylene," Appl. Opt. **53**, 731–735 (2014).
9. N. B. Hébert, V. Michaud-Belleau, J. D. Anstie, J.-D. Deschênes, A. N. Luiten, and J. Genest, "Self-heterodyne interference spectroscopy using a comb generated by pseudo-random modulation," Opt. Express **23**, 27806–27818 (2015).
10. N. B. Hébert, V. Michaud-Belleau, C. Perrella, G.-W. Truong, J. D. Anstie, T. M. Stace, J. Genest, and A. N. Luiten, "Real-time dynamic atomic spectroscopy using electro-optic frequency combs," Phys. Rev. Appl. **6**, 044012 (2016).
11. N. Wilson, N. B. Hébert, C. Perrella, P. Light, J. Genest, S. Pustelny, and A. Luiten, "Simultaneous observation of nonlinear magneto-optical rotation in the temporal and spectral domains with an electro-optic frequency comb," Phys. Rev. Appl. **10**, 034012 (2018).
12. D. A. Long, A. J. Fleisher, D. F. Plusquellic, and J. T. Hodges, "Multiplexed sub-doppler spectroscopy with an optical frequency comb," Phys. Rev. A **94**, 061801 (2016).
13. D. A. Long, A. J. Fleisher, D. F. Plusquellic, and J. T. Hodges, "Electromagnetically induced transparency in vacuum and buffer gas potassium cells probed via electro-optic frequency combs," Opt. Lett. **42**, 4430–4433 (2017).
14. I. Coddington, N. Newbury, and W. Swann, "Dual-comb spectroscopy," Optica. **3**, 414–426 (2016).
15. N. B. Hébert, J. Genest, J.-D. Deschênes, H. Bergeron, G. Y. Chen, C. Khurmi, and D. G. Lancaster, "Self-corrected chip-based dual-comb spectrometer," Opt. Express **25**, 8168–8179 (2017).
16. D. A. Long, A. J. Fleisher, K. O. Douglass, S. E. Maxwell, K. Bielska, J. T. Hodges, and D. F. Plusquellic, "Multiheterodyne spectroscopy with optical frequency combs generated from a continuous-wave laser," Opt. Lett. **39**, 2688–2690 (2014).
17. P. Guay, J. Genest, and A. J. Fleisher, "Precision spectroscopy of h13cn using a free-running, all-fiber dual electro-optic frequency comb system," Opt. Lett. **43**, 1407–1410 (2018).
18. I. E. Gordon, L. S. Rothman, C. Hill, R. V. Kochanov, Y. Tan, P. F. Bernath, M. Birk, V. Boudon, A. Campargue, K. Chance *et al.*, "The hitran2016 molecular spectroscopic database," J. Quant. Spectrosc. Radiat. Transf. **203**, 3–69 (2017).